

## Template assisted self-assembly of iron oxide nanoparticles: An x-ray structural analysis

D. Mishra, H. Zabel, S. V. Ulyanov, V. P. Romanov, and V. M. Uzdin

Citation: [Journal of Applied Physics](#) **115**, 054104 (2014); doi: 10.1063/1.4864129

View online: <http://dx.doi.org/10.1063/1.4864129>

View Table of Contents: <http://scitation.aip.org/content/aip/journal/jap/115/5?ver=pdfcov>

Published by the [AIP Publishing](#)

---

### Articles you may be interested in

[Self organization of magnetic nanoparticles: A polarized grazing incidence small angle neutron scattering and grazing incidence small angle x-ray scattering study](#)

*J. Appl. Phys.* **110**, 102207 (2011); 10.1063/1.3661654

[Structure and optical properties of self-assembled multicomponent plasmonic nanogels](#)

*Appl. Phys. Lett.* **99**, 043112 (2011); 10.1063/1.3615785

[Structural study of self-assembled Co nanoparticles](#)

*J. Appl. Phys.* **94**, 7743 (2003); 10.1063/1.1627953

[Self-assembled gradient nanoparticle-polymer multilayers investigated by an advanced characterization method: microbeam grazing incidence x-ray scattering](#)

*Appl. Phys. Lett.* **82**, 1935 (2003); 10.1063/1.1563051

[Self-assembled patterns of iron oxide nanoparticles by hydrothermal chemical-vapor deposition](#)

*Appl. Phys. Lett.* **79**, 4207 (2001); 10.1063/1.1426256

---



## Template assisted self-assembly of iron oxide nanoparticles: An x-ray structural analysis

D. Mishra,<sup>1,5</sup> H. Zabel,<sup>1</sup> S. V. Ulyanov,<sup>2,3</sup> V. P. Romanov,<sup>2</sup> and V. M. Uzdin<sup>2,4</sup>

<sup>1</sup>*Department of Physics, Ruhr-University Bochum, 44780 Bochum, Germany*

<sup>2</sup>*St.-Petersburg State University, Ul'yanovskaya ul.1, Petrodvorets, St.-Petersburg 198904, Russia*

<sup>3</sup>*St.-Petersburg University of Commerce and Economics, St.-Petersburg 194018, Russia*

<sup>4</sup>*St.-Petersburg National Research University of Information Technologies, Mechanics and Optics, 49, Kronverkskij, St.-Petersburg 197101, Russia*

<sup>5</sup>*Institut fuer Optik und Atomare Physik, Technische Universitaet Berlin, Strasse des 17. Juni 135, 10623 Berlin, Germany*

(Received 10 September 2013; accepted 22 January 2014; published online 6 February 2014)

We have fabricated by e-beam lithography periodic arrays of rectangular shaped trenches of different widths into Si substrates. The trenches were filled with iron oxide nanoparticles, 20 nm in diameter, by spin-coating them onto the Si substrate. The trenches have the purpose to assist the self-assembly of the iron oxide nanoparticles. Using x-ray scattering techniques, we have analyzed the structure factor of the trenches before and after filling in order to determine the filling factor. We present a theoretical analysis of the x-ray scattering function within the distorted-wave Born approximation and we present a quantitative comparison between theory and experiment. © 2014 AIP Publishing LLC. [<http://dx.doi.org/10.1063/1.4864129>]

### I. INTRODUCTION

Nanoparticles (NPs) (often also termed nanocrystals or nanoclusters) attract much interest because of their numerous already realized or anticipated applications ranging from photonic and spintronic devices to bio-medical functionalities.<sup>1</sup> For some applications, self-assembly of NPs into ordered crystalline like structures forming close packed monolayers or multilayers is essential. However, for a successful NP self-assembly, some control or assistance is required.<sup>2</sup> Without templates, the close packed NP layers usually contain topological defects, such as vacancies, dislocations, and disclinations, which reduce the structural coherence length.<sup>3</sup> With defects, control over the exact location of NPs is impeded. Assisted self-assembly of NPs is a promising route to remedy this problem. There are several approaches for assisted self-assembly. Usually, a regular template is provided, which defines the long range structure. This can be done, for instance, by the use of a nanostructured aluminum template prepared by an anodization process,<sup>4</sup> or by using lithographically prepared templates of rectangular stripes.<sup>5</sup> Templates can also be prepared by self-assembly of di-block copolymers (DBC),<sup>6</sup> nanoparticles,<sup>7</sup> or DNA.<sup>8</sup> The templates are then covered with NPs using a spreading drop technique or by a spin-coating process. The main idea is to direct the self-assembly within desired structures to reduce defects and vacancies.

In the following, we will consider templates consisting of an array of rectangular trenches etched into a Si substrate. Subsequently, the trenches are filled with iron-oxide NPs via spin-coating. We have performed x-ray scattering experiments for the structural analysis of these assemblies. From the scattering experiments, we want to learn about the filling factor of the trenches. This information cannot be gained by other experimental techniques such as imaging with scanning electron microscopy (SEM), atomic force

microscopy (AFM), or scanning tunneling microscopy (STM) because of lack of depth sensitivity. But SEM will be used for the pre-characterization of our structures before and after spin-coating. For investigating the ordering of the NPs, grazing incidence small angle x-ray scattering (GISAXS) has been used and this was reported elsewhere.<sup>9</sup> Here, we concentrate on the average electron density profile, which is recorded by off-specular reflectivity scans, so called transverse scans or rocking scans at small glancing angles of the incident beam. It has been shown that it is possible to determine the layering and ordering of fluids and colloidal suspensions confined within micro channel arrays by synchrotron radiation in transmission geometry.<sup>10,11</sup> Linear arrays of rectangular channels act as a diffraction grating. Comparing the diffracted intensities from filled to empty channels, the phase shift due to the fluid was calculated, from which the refractive index and the volume fraction of the confined fluid was deduced. Our experimental approach is similar, but also has many differences. We measure in a reflection geometry. The trenches are filled with NPs, without any fluids. Hence, our aim is to find out the filling factor of NPs and to reduce structural defects compared to a continuous monolayer film. The theoretical model is also different from that of Ref. 10. A scattering theory for the analysis of lateral arrays in reflection geometry has also been reported in the literature before in the Born approximation, in the Distorted Wave Born Approximation (DWBA), and using dynamical theory of x-ray diffraction.<sup>12–15</sup> Here, we use the DWBA approach, which has been widely applied for describing the x-ray scattering on lateral structures.<sup>16</sup> The DWBA approach is relatively simple and even in the first-order gives a good qualitative description of the experimental data.

This contribution is organized as follows. In Section II, the preparation of the template, filling with NPs, and x-ray

characterization is described. In section III follows a detailed theoretical analysis with the goal to describe the experimental data and to gain information about the filling of the NPs in the trenches.

## II. EXPERIMENTAL PROCEDURES AND RESULTS

### A. Template preparation

The templates were prepared on silicon (100) substrates cut into a size of 10 mm × 10 mm covered with a native silicon dioxide purchased from CrysTech. The substrates were cleaned in acetone and isopropanol for 10 min inside an ultrasonic bath and dried by a jet of nitrogen gas.

Electron beam lithography (EBL) was used to create trenches or channels into the Si substrate of 120 nm width and a periodicity  $l = 1.3 \mu\text{m}$ , with an aspect ratio (length to width) of the order of 400, and a depth that depends on the etching time. For EBL, we used a modified Quanta 200 FEG SEM equipped with a Raith ELPHY Quantum lithography attachment.

The EBL protocol for obtaining trenches of the desired dimensions consists of 6 steps schematically shown in Figure 1 as a side view. The sequences are as follows:

- Step 1: Spin-coating of polymethyl methacrylate (PMMA) on silicon and baking at 170°C in air for 10 min.
- Step 2: Exposure to electron beam (structures are created by GDSII software from Raith lithography).
- Step 3: Developing the film in Methyl isobutyl ketone (MIBK) and isopropanol solution.
- Step 4: Etching by Ar ions in a vacuum chamber (removal of remaining PMMA).
- Step 5: Spin-coating NPs.
- Step 6: Removal of PMMA by washing in acetone and drying with nitrogen gas.

Polymethyl methacrylate 200k with 4% dilution in chlorobenzene was used as positive photoresist in the EBL process. Approximately, 5 ml of the solution was spin-coated at 4000 revolution per minute (rpm) for 30 s. The spin-coated PMMA sample was then baked at 170°C for 10 min on a hot plate. This sample was inserted inside the SEM chamber to write the patterns by EBL. The patterns were created by GDSII database provided by ELPHY software. After exposure, the sample was developed in a solution of MIBK and isopropanol

mixed in a ratio 1:3. Isopropanol was used as a stopper (to stop the development). The development time was varied between 30 s and 4 min until the patterns were clearly visible under an optical microscope. The sample was dipped in the stopper for 30 s after development. The etching as shown in step 4 is necessary to remove residual PMMA completely from the exposed regions, which was left over after the development. The etching was performed by ion beam sputtering (Roth and Rau) in an Ar plasma at  $1.5 \times 10^{-3}$  mbar for 240 s. During the etching time usually a shallow trench is formed inside the silicon substrate. Depending on the time of etching the depth can be varied. We used two different etching times, 240 s (s\_etch for short etching time or shallow etch) and 480 s (d\_etch for long etching time or deeper etch).

The NPs consist of chemically synthesized iron oxide (purchased from Ocean NanoTech LLC) of 20 nm diameter with 6.5% size distribution. The NPs are covered with an oleic acid shell and are dispersed in toluene. They were spin-coated on silicon (100) substrates containing the EBL defined patterns. Spin-coating usually leads to a uniform coverage of the entire substrate. However, because of the existence of trenches, in the present case, the NPs preferentially assemble inside of the trenches. The films are heat-treated at 80°C in air on a hot plate to remove the excess solvent. Further heat treatments up to 230°C in vacuum lead to a change in the crystalline phase of the iron oxide without affecting the particle ordering in the film. Further details of sample preparation and magnetic characterizations are reported in Ref. 17.

Figure 2 shows SEM images of trenches coated with NPs filling about 5 to 6 particles across the channel. Most likely, the number of layers is more than one, but this filling factor has to be determined from an accurate fit to the intensity of the x-ray satellite peaks, see Secs. II B and III. Figure 2(b) shows the trenches at a lower magnification and therefore the periodicity of the trenches becomes visible in the field of view. Figures 2(c) and 2(d) show trenches without NPs (empty trenches). The empty trenches are used as reference substrates for x-ray scattering experiments.

In order to obtain sufficient x-ray intensity in the satellite reflections that can be distinguished from the background intensity, a large number of channels are required. Therefore, one needs to prepare by EBL, an extended periodic pattern over an area of at least a few millimeters. Large area scanning

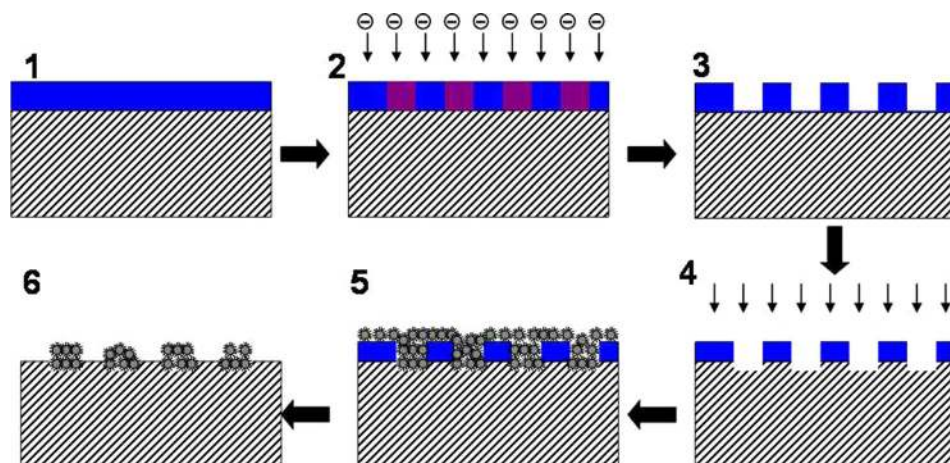


FIG. 1. The schematic of the lithographic process used to fabricate trenches of 130 nm widths. Different steps are explained in the text.

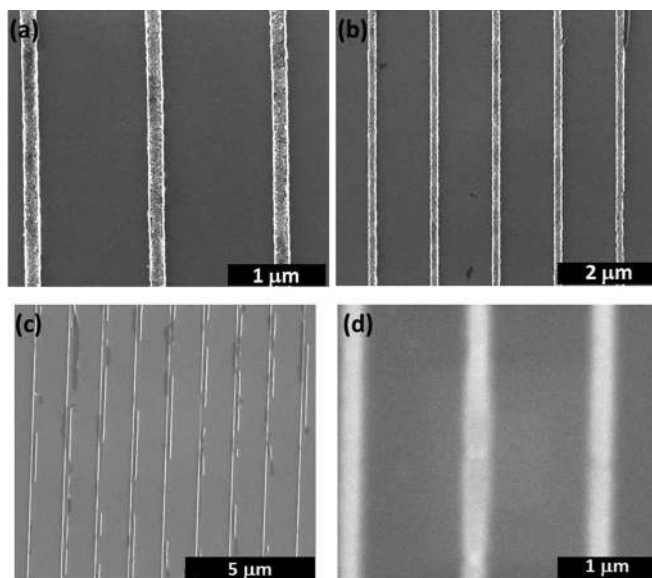


FIG. 2. SEM images of lithographically prepared trenches. (a) and (b) show the trenches filled with NPs. (c) and (d) show the empty trenches without NPs. The width of the trenches is 130 nm and the periodicity is 1.3  $\mu\text{m}$ . The broken bright lines in (c) arise due to residual PMMA left due to incomplete removal during development and etching process.

Laser lithography or UV mask techniques cannot be used because of inadequate resolution. On the other hand, for the definition of narrow trenches of only 100 nm width, a well-focused electron beam is required for scanning across the PMMA surface.<sup>18</sup> The higher the e-beam resolution and the sharper the focus, the smaller is the range of the scan. As a good compromise between resolution and scanning range, we chose a writing field of 50  $\mu\text{m} \times 50 \mu\text{m}$ , which contains roughly 50 channels. Then, the writing fields were stitched together to cover a total area of 8 mm  $\times$  8 mm on a 10 mm  $\times$  10 mm Si substrate. The stitching cannot be done seamlessly because of backlash problems of the motorized sample stage in the SEM. Therefore, it is safer to leave a gap between each writing field. The total area was actually divided into four smaller squares each of 2 mm  $\times$  2 mm patches containing 20  $\times$  20 writing fields of 50  $\mu\text{m} \times 50 \mu\text{m}$  each. Figure 3 shows a representative series of SEM images from low magnification to higher magnification. Figure 3(a) shows the total area covering many writing fields over the total area of 8 mm  $\times$  8 mm. Some regions have no structures due to improper focusing or lower exposure time of the electron beam. The bottom left and top right side parts show a better definition of the structures than the other two parts. Figure 3(b) is a magnification of the top left part in Fig. 3(a). Still some defects can be recognized in this SEM image. The writing fields are not equidistant from each other and there are certain places, where the writing field is completely missing. This latter error is due to a software mistake. Figure 3(c) shows one of the writing fields containing 50 channels forming continuous lines equidistant from each other. In the rocking scans, the periodicity of these trenches are probed, which is of the order of 1.25  $\mu\text{m}$ . There are some defects in the trenches as well, such as discontinuity and edge roughness. This depends on the local chemical nature of the PMMA polymer during development and subsequent removal of the

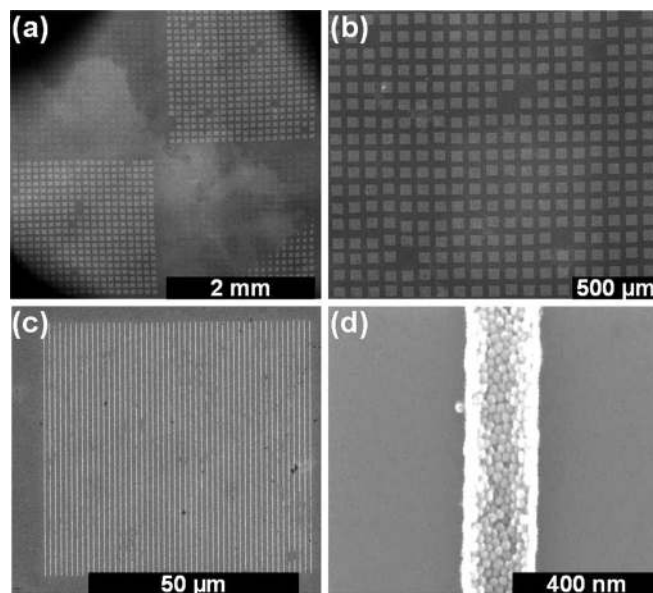


FIG. 3. SEM images of a series of lithographically prepared trenches from lower magnification to higher magnification. (a) The whole substrate covered with many square like patterns, which contains the nanostructures. (b) One of the areas containing many writing fields. (c) One of the writing fields (patches) containing several trenches or nanostructures. (d) One nanostructure or trench filled with NPs.

PMMA in the final step. Figure 3(d) shows one of the trenches containing NPs inside it. The NPs are close-packed similar to a film with several layers but essentially no vacancies, which was the aim of the exercise.

## B. X-ray characterization

To probe the periodicity of the channels in the pattern and to determine the filling factor of the NPs inside the trenches, rocking scans ( $q_x$ -scans) were performed in reflection geometry. The experiments were performed at the HASYLAB, DESY, Hamburg using beamline W1 with a photon energy of 11 keV ( $\lambda = 0.1127 \text{ nm}$ ) and 8.047 keV ( $\lambda = 0.1541 \text{ nm}$ ). The rocking scans may also be characterized as off-specular reflectivity scans at small glancing angle  $\alpha_i$  of the incident x-ray beam, directed perpendicular to the trenches. During the off-specular scan, the detector position is held fixed at  $\alpha_i + \alpha_f$  and the incident angle was scanned from 0 to  $\alpha_i + \alpha_f$  with a step size of 0.005°. In this scan, the in-plane periodic pattern is investigated by the  $q_x$  component (x-component) of the scattering vector  $\mathbf{q}$ , given by the following equation:

$$q_x = \frac{2\pi}{\lambda} (\cos \alpha_f - \cos \alpha_i),$$

where  $\alpha_i$  is the angle of incidence and  $\alpha_f$  is the angle of reflection. The specular condition is satisfied for  $\alpha_i = \alpha_f$ . The constant detector position also ensures that  $\alpha_i + \alpha_f$  always remains constant during the off-specular scan. In the rocking scan, only the direction of the scattering vector  $\mathbf{q}$  changes (length remains constant). When  $q_x = \pm 2\pi/l$ , a satellite peak appears on both sides of the specular reflected beam, where  $l$  is the lateral periodicity. Figures 4(a) and 4(b) show the specular and the rocking scans geometry, respectively. The

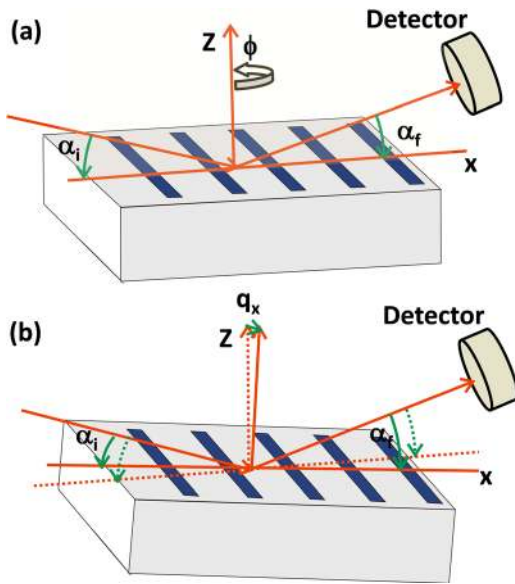


FIG. 4. Geometry for rocking scan. (a) Condition for specular scan. ( $\alpha_i = \alpha_f$ ). The rotation about the surface normal is given by  $\phi$ , which shows whether the trenches are parallel or perpendicular to the scattering plane  $xz$  (shaded rectangle). (b) Condition for rocking scans ( $\alpha_i \neq \alpha_f$ ). The detector position is always fixed and is given by  $\alpha_i + \alpha_f$ . The  $q_x$  component of the scattering vector  $\mathbf{q}$  scans the lateral periodicity.

length of  $|\mathbf{q}|$  remains constant, only the component  $q_x$  is obtained by tilting the sample as shown in Figure 4(b). In this coordinate system, the  $z$ -component is perpendicular to the sample surface, the  $x$ -component is in the scattering plane and perpendicular to  $z$ , and the  $y$ -component is perpendicular to the scattering plane. The periodic array of trenches with periodicity  $l$  is parallel to the  $y$ -component or perpendicular to the scattering plane ( $xz$  plane). The rotation around the  $z$ -axis is given by  $\phi$ , which shows whether the trenches are parallel ( $\phi = 90^\circ$ ) or perpendicular ( $\phi = 0^\circ$ ) to the  $x$ -ray beam direction. The experimentally observed intensities are always normalized to the monitor counts for comparison.

The complete x-ray scattering theory is provided in Sec. III. The peak intensity takes into account the lattice disorder, which appears due to roughness of the trenches, the width variation from EBL processing, and variations of the NP packing inside the trenches.

### C. Experimental results

Figure 5 shows an off-specular reflectivity scan of the patterned sample with the trenches aligned perpendicular to the scattering plane ( $xz$  plane,  $\phi = 0^\circ$ ) and a scan with the trenches oriented parallel to scattering plane ( $xz$  plane,  $\phi = 90^\circ$ ). In this figure, it can clearly be recognized that the off-specular satellite peaks are only visible if the component of the scattering vector  $q_x$  is oriented perpendicular to the trenches, as one would expect. The intensity of the side peaks is actually very sensitive to the proper alignment of the sample. In the following scans are shown with optimized alignments only. Under optimized conditions, the intensity of the satellite peaks is almost three orders of magnitude lower than the specularly reflected intensity at  $q_x = 0$ .

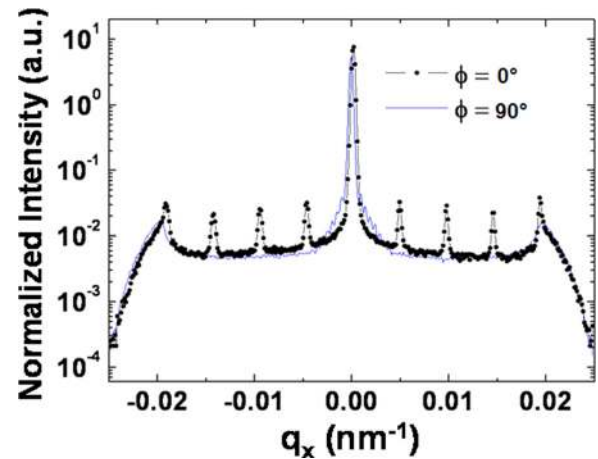


FIG. 5. Rocking scans of template assisted self-assembled NPs. Rocking scan measured at  $2^\circ$  of detector angle. Trenches are oriented parallel (blue solid line,  $\phi = 90^\circ$ ) and perpendicular (black solid circles,  $\phi = 0^\circ$ ) to the scattering plane. The orientation is defined by angle  $\phi$  ( $x$ -ray wavelength of  $\lambda = 0.1541$  nm).

The scans shown in Figure 5 are taken with a detector angle at  $2^\circ$  and  $x$ -ray wavelength of  $\lambda = 0.1541$  nm. From the position of the satellite peaks, the periodicity can be calculated using the following equation:

$$l = \frac{2\pi}{\Delta q_x},$$

where  $\Delta q_x$  is the separation between the satellite peaks. The periodicity obtained from the above equation is  $l = 2\pi/0.005 \text{ nm}^{-1}$  or  $l = 1.256 \mu\text{m}$ , which matches well with the SEM observations. The 4th order peak directly sits on top of the Yoneda position, which is defined by the coincidence of either  $\alpha_i$  or  $\alpha_f$  with the critical angle  $\alpha_c$  for  $x$ -ray total reflection. These measurements also show that in spite of the irregular arrangement of the writing fields or patches, the channels (trenches) within individual writing fields are well ordered. The  $x$ -ray intensity detected is an incoherent sum over all coherently illuminated areas, which may comprise more than one patch at the shallow scattering angles used.

In order to compare the NP arrangement inside the trenches, rocking scans of structures with and without NPs were compared. Figure 6(a) shows the comparison of samples filled with NPs and without NPs at a detector angle  $2^\circ$ . Figure 6(b) shows the comparison of rocking scans for detector angles  $1^\circ$ ,  $1.6^\circ$ ,  $2^\circ$ , and  $3^\circ$ , respectively, measured at  $\lambda = 0.1127$  nm. With increasing the detector angle from  $1^\circ$  to  $2^\circ$  higher order satellite peaks are captured by increasing the  $q_x$  range. But increasing the detector angle further to  $3^\circ$  degrades the quality of the scan. Surprisingly, there is no intensity difference between samples with NPs and without NPs. The trenches with NPs have higher scattering volume (containing iron oxides) compared to empty trenches (containing only air). But no difference in intensities were observed for all rocking scans. The simulations described in Sec. III provide a complete account on this remarkable anomaly. In short, equal intensity before and after filling the trenches with FeO NPs is met for a volume fraction of about

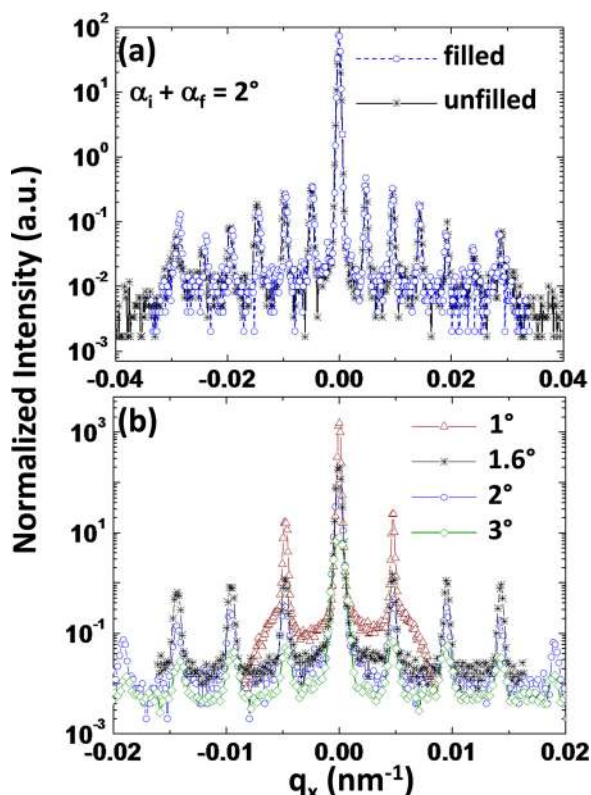


FIG. 6. Rocking scans of template assisted self-assembled NPs. (a) Rocking scan measured at  $2^\circ$  of detector angle with trenches filled with NPs (open circle) and trenches without NPs (stars). (b) Rocking scans measured at  $1^\circ$ ,  $1.6^\circ$ ,  $2^\circ$ , and  $3^\circ$  detector angles, respectively, for samples with NPs. X-ray wavelength  $\lambda = 0.1127$  nm.

65%. This corresponds to a close packed and complete filling of the trenches with packing density of 65%, the same density that is also observed for FeO NPs spin-coated on plane Si substrates.<sup>9</sup> The peak intensity decreases with increasing order. But peaks on top of the Yoneda wings always have higher intensity compared to its previous order peak, which is to be expected from the diffraction theory.<sup>19</sup>

Figures 7(a) and 7(b) show rocking scans performed at another two detector angles of  $1.6^\circ$  and  $3^\circ$ , respectively. The intensities of satellite peaks for trenches filled with NPs and without NPs follow a similar trend like measurements done at a detector angle of  $2^\circ$ .

In case of trenches without NPs, two sets of samples were prepared, one, with long etching time of 480 s and hence with a deeper depth (d\_etch) and the other with short etching time of 240 s and smaller depth (s\_etch). The etching corresponds to the step 4 in the trench preparation process. Figures 8(a) and 8(b) show the comparison of rocking scans measured at  $1.6^\circ$  and  $3^\circ$ , respectively, for samples without NPs with different etching times. One property, which is quite distinguished in these patterns, is the fact that satellite peak intensities for the long etched substrate without NPs (d\_etch) are lower than for the short etched substrate without NPs (s\_etch). Probably, the longer etching time leads to a rougher surface and hence to a decrease in the satellite peak intensity.

The resolution along  $q_x$  is not sensitive enough to resolve the ordering of NPs, within individual trenches as it

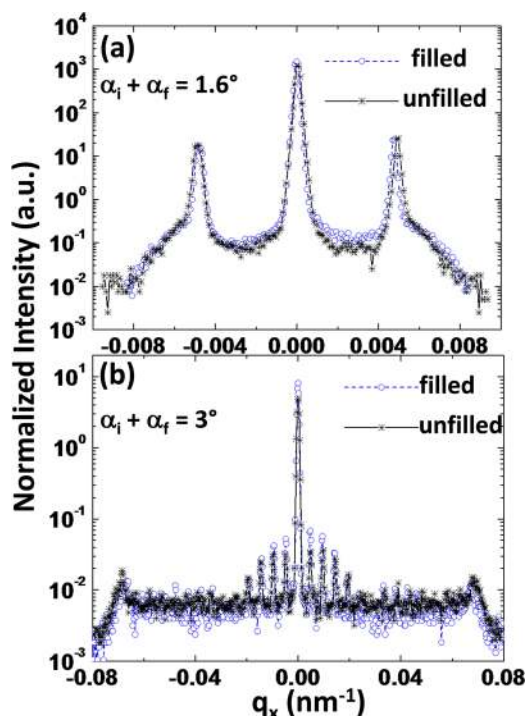


FIG. 7. Rocking scans of the trenches measured at detector angle (a)  $1.6^\circ$  and (b)  $3^\circ$  with trenches filled with NPs (open circles), trenches without NPs (stars). X-ray wavelength  $\lambda = 0.1127$  nm.

would be possible with GISAXS measurements.<sup>9</sup> So it is difficult to estimate the quality of ordering of NPs within the trenches from the rocking scans alone. In the  $q_x$  scans, the lateral (in-plane) electron or charge scattering length density (cSLD) variation is probed. The periodic variation created

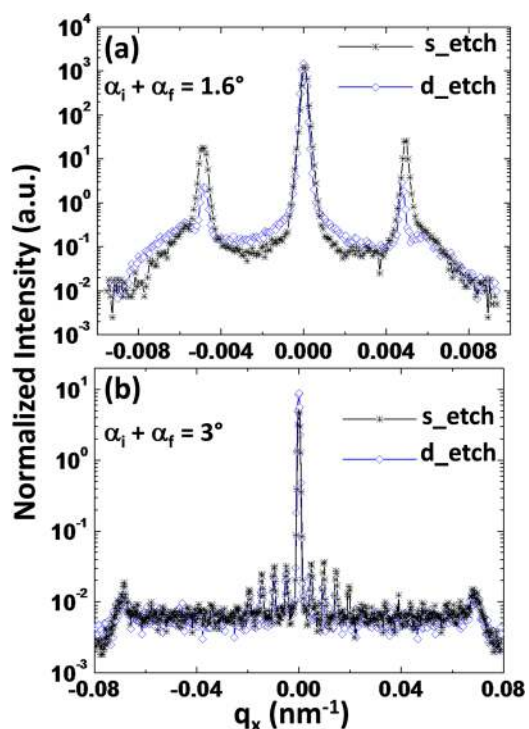


FIG. 8. Rocking scans of the trenches measured at (a)  $1.6^\circ$  and (b)  $3^\circ$  without NPs, having a shallow depth (s\_etch, stars) and deep depth (d\_etch, diamonds). X-ray wavelength  $\lambda = 0.1127$  nm.

by the trenches generates the satellite peaks. This will quantitatively be determined for empty and filled trenches in Section III.

### III. THEORY

#### A. X-ray scattering on structures with trenches filled with nanoparticles

We will consider x-ray scattering of a rough surface with parallel rectangular trenches located at the surface. The trenches can either be empty or filled with another substance, such as nanoparticles. The reflection coefficient of the x-ray radiation from such a system is calculated in the frame of the DWBA approach.

For a monochromatic wave, with time dependence determined by the factor  $e^{-i\omega t}$ , we have

$$(\Delta + k^2 \varepsilon(\mathbf{r}))\mathbf{E}(\mathbf{r}) = -\nabla((\nabla \ln \varepsilon(\mathbf{r})) \cdot \mathbf{E}(\mathbf{r})), \quad (1)$$

where  $\Delta$  is the Laplace operator,  $k = |\mathbf{k}| = \frac{\omega}{c}$  is the wave vector, and  $c$  is the velocity of light in vacuum. The calculations will be carried out in a Cartesian coordinate system, defined already in Sec. II B. The plane  $z=0$  corresponds to the unperturbed surface of the substrate,  $z$ -axis is directed into the vacuum, and the trenches are parallel to the  $y$ -axis. Consider the scattering of the wave incident on the sample in  $xz$ -plane with polarization along the  $y$ -axis. The permittivity  $\varepsilon$  and the refractive index  $n$  at x-ray frequencies are close to unity and their real parts are less than unity

$$n = 1 - \delta + i\beta, \quad \varepsilon \approx 1 - 2\delta + 2i\beta, \quad \ln \varepsilon(\mathbf{r}) \approx -2\delta + 2i\beta. \quad (2)$$

In this case, taking into account that the correlation length for  $\varepsilon(\mathbf{r})$  is much larger than the x-ray wavelength, we can neglect the right hand side of Eq. (1). Then, Eq. (1) becomes a scalar one

$$(\Delta + k^2 \varepsilon(\mathbf{r}))E(\mathbf{r}) = 0. \quad (3)$$

It is convenient to divide the permittivity  $\varepsilon(\mathbf{r})$  into three parts

$$\varepsilon(\mathbf{r}) = \bar{\varepsilon}(\mathbf{r}) + \delta\varepsilon_{reg}(\mathbf{r}) + \delta\varepsilon_{rough}(\mathbf{r}), \quad (4)$$

where  $\bar{\varepsilon}(\mathbf{r})$  is the permittivity of the ideal system with a flat substrate-vacuum interface

$$\bar{\varepsilon}(\mathbf{r}) = \theta(z) + \varepsilon_s \theta(-z), \quad (5)$$

where  $\theta(z)$  is the Heaviside function and  $\varepsilon_s$  is the permittivity of the substrate.

The part  $\delta\varepsilon_{reg}(\mathbf{r})$  takes into account the existence of empty or filled trenches by another substance at the surface, whereas  $\delta\varepsilon_{rough}(\mathbf{r})$  is determined by random surface roughness. For empty parallel trenches on the substrate surface, we have

$$\delta\varepsilon_{reg}(\mathbf{r}) = \Delta \varepsilon [\theta(z+h) - \theta(z)] \sum_{m=1}^M [\theta(x-x'_m) - \theta(x-x''_m)], \quad (6)$$

where  $\Delta \varepsilon = \varepsilon_s - 1$ ,  $x'_m = (m-1)l$ ,  $x''_m = (m-1)l + a$ ,  $h$  is the depth,  $a$  is the width of the trenches,  $l$  is the periodicity of the trench pattern, and  $M$  is the number of trenches in the correlated area. If the trenches are filled with a material having permittivity  $\varepsilon_{np} \approx 1 - 2\delta_{np} + 2i\beta_{np}$ , then in (6) should be used  $\Delta \varepsilon = \varepsilon_s - \varepsilon_{np}$ .

In the DWBA approach, the scattered field at point  $\mathbf{r}$ ,  $E(\mathbf{r})$  is the sum of three terms

$$E(\mathbf{r}) = E_{Fr}(\mathbf{r}) + E_{reg}(\mathbf{r}) + E_{rough}(\mathbf{r}), \quad (7)$$

where  $E_{Fr}(\mathbf{r})$  is the Fresnel solution for a perfectly flat interface,  $E_{reg}(\mathbf{r})$  is the field associated with the presence of empty or filled with other material trenches,  $E_{rough}(\mathbf{r})$  is the random field due to the scattering from substrate roughness. For the first term, which describes the scattering of a monochromatic plane wave on a perfectly flat interface, we have

$$E_{Fr}(\mathbf{r}) = E_0(\mathbf{r}) + k^2 \int d\mathbf{r}' G(\mathbf{r}, \mathbf{r}') [1 - \bar{\varepsilon}(\mathbf{r}')] E_0(\mathbf{r}'), \quad (8)$$

where  $E_0(\mathbf{r}) = e^{i\mathbf{k}\cdot\mathbf{r}}$  is the field of the incident wave, the amplitude of which is assumed to be unit,  $\mathbf{k}$  is the wave vector of the incident wave,  $G(\mathbf{r}, \mathbf{r}')$  is the Green's function, which satisfies the equation

$$(\Delta + k^2 \bar{\varepsilon}(\mathbf{r}))G(\mathbf{r}, \mathbf{r}') = \delta(\mathbf{r} - \mathbf{r}'), \quad (9)$$

and the radiation condition. Here,  $\delta(\mathbf{r})$  is the  $\delta$ -function.

The second and third terms in (7) are given by

$$E_{reg}(\mathbf{r}) = -k^2 \int d\mathbf{r}' G(\mathbf{r}, \mathbf{r}') \Delta \varepsilon_{reg}(\mathbf{r}') E_{Fr}(\mathbf{r}') \quad (10)$$

and

$$E_{rough}(\mathbf{r}) = -k^2 \int d\mathbf{r}' G(\mathbf{r}, \mathbf{r}') \Delta \varepsilon_{rough}(\mathbf{r}') E_{Fr}(\mathbf{r}'). \quad (11)$$

In scattering problems, for  $r \gg D$ , where  $D$  is the characteristic size of the sample, for the Green function, one can use the far zone approximation. Then, the Green function can be written as

$$G(\mathbf{r}, \mathbf{r}') = -\frac{e^{ikr}}{4\pi r} \mathfrak{S}_{Fr}(\mathbf{r}', -\mathbf{k}_{sc}), \quad (12)$$

where  $\mathfrak{S}_{Fr}(\mathbf{r}', -\mathbf{k}_{sc})$  is the solution of Fresnel problem for plane waves with unit amplitude  $e^{-i\omega t - i\mathbf{k}_{sc}\cdot\mathbf{r}'}$ , where  $\mathbf{k}_{sc} = k \frac{\mathbf{r}}{r}$  is the wave vector of the scattered wave.

For scattering on an ideally flat boundary,  $E_{Fr}(\mathbf{r})$  can be written as

$$E_{Fr}(\mathbf{r}) = E_0(\mathbf{r}) + (2\pi)^2 \delta(\mathbf{q}_{\perp}) \Delta \varepsilon \frac{iT'}{q_{1,z}^0} \frac{k^2}{4\pi} \frac{e^{ikr}}{r}, \quad (13)$$

where the scattering vector is defined as  $\mathbf{q} = \mathbf{k} - \mathbf{k}_{sc}$ , and the vector  $\mathbf{q}_{\perp}$  is the component of the scattering vector in the plane of the interface,  $q_{1,z}^0 = k(\sqrt{\varepsilon_s - \cos^2 \alpha_f} + \sin \alpha_i)$ . The value  $T'$  is the amplitude of the field inside the substrate

at the surface, arising due to a wave of unit amplitude that falls from vacuum on the interface at an angle of  $\alpha_f$ .

In the general case, the angle between the wave vector of the incident wave and the direction of the trenches on the surface can be arbitrary. Denote via  $\phi_i$  the angle between  $xz$ -plane, perpendicular to the trenches and the plane perpendicular to the substrate, which contains the incident beam. The scattering plane may not be perpendicular to the substrate surface and we denote via  $\phi_f$  the angle between the  $xz$ -plane and the plane perpendicular to substrate, which contains the scattered beam.

The total field  $E(\mathbf{r})$  is obtained from (7) by a straightforward calculation

$$E(\mathbf{r}) = E_0(\mathbf{r}) + \frac{k^2}{4\pi} \frac{e^{ikr}}{r} (\alpha + A + B), \quad (14)$$

where

$$\begin{aligned} \alpha &= (2\pi)^2 \delta(\mathbf{q}_\perp) \Delta \varepsilon \frac{iT'}{q_{1,z}}, \\ A &= -8\pi \Delta \varepsilon T T' \delta(q_y) \frac{\sin \frac{q_{1,z} h}{2}}{q_{1,z}} e^{i \frac{q_{1,z} h}{2}} e^{-i q_x \frac{(M-1)l+a}{2}} \\ &\quad \times \frac{\sin \frac{q_x a}{2}}{q_x} \frac{\sin \frac{q_x M l}{2}}{\sin \frac{q_x l}{2}}, \\ B &= \Delta \varepsilon T T' \frac{i}{q_{1,z}} \int d\mathbf{r}_\perp e^{-i \mathbf{q}_\perp \cdot \mathbf{r}_\perp} (e^{-i q_{1,z} u(\mathbf{r}_\perp)} - 1). \end{aligned}$$

Here,  $q_{1,z} = k(\sqrt{\varepsilon_s - \cos^2 \alpha_f} + \sqrt{\varepsilon_s - \cos^2 \alpha_i})$ ,  $T$  is the amplitude of the field inside the substrate at the surface caused by the wave of unit amplitude that falls from vacuum on the interface at an angle of  $\alpha_i$ ,  $u(\mathbf{r}_\perp)$  is the random deviation of  $z$ -coordinate of the real interface relative to the plane  $z = 0$ . It is assumed that  $\langle u \rangle = 0$  after averaging over the entire sample surface. The reflection coefficient  $R$  is defined as the ratio of the x-ray scattered intensity into the solid angle  $\Delta\Omega$ , which depends on the angular aperture of the detector and the intensity of the incident radiation. It can be expressed as a sum of two terms

$$R = R_{reg} + R_{diff}. \quad (15)$$

The first term describes the scattering at the interface without random roughness, but with regular trenches, empty or filled with another substance, and the second term describes the contribution to the diffuse scattering, which arises because of the random roughness

$$R_{reg} = \frac{1}{S \sin \alpha_i} \frac{k^4}{16\pi^2} \int_{\Delta\Omega} d\Omega |\alpha + A + \langle B \rangle|^2, \quad (16)$$

$$R_{diff} = \frac{1}{S \sin \alpha_i} \frac{k^4}{16\pi^2} \int_{\Delta\Omega} d\Omega (\langle |B|^2 \rangle - |\langle B \rangle|^2). \quad (17)$$

Here,  $S$  is the illuminated area,  $d\Omega = \frac{dq_x dq_y}{k^2 \sin \alpha_f}$ ,  $\langle B \rangle = \Delta \varepsilon T T' \frac{i}{q_{1,z}} \delta(\mathbf{q}_\perp) (e^{-\frac{q_{1,z}^2 \sigma^2}{2}} - 1)$ . It is assumed that the roughness fluctuations have a Gaussian form;  $\sigma$  is the root mean square (RMS) roughness of the interface.

The diffraction pattern is generated by the term  $|A|^2$ , which contains the function

$$\Phi(q_x) = \frac{\sin^2 \frac{q_x L_x}{2}}{\sin^2 \frac{q_x l}{2}}, \quad (18)$$

where  $L_x = Ml \gg l$ . This function is periodic:  $\Phi(q_x) = \Phi(q_x + \frac{2\pi}{l})$ . For large  $M$ , the peaks of  $\Phi(q_x)$  are very sharp. Diffraction peaks should be observable when the following conditions for the components of the scattering vector are satisfied

$$\begin{cases} q_y = 0 \\ q_x = q_p, \end{cases} \quad (19)$$

where  $q_p = \frac{2\pi}{l} p$ ,  $p = 0, \pm 1, \pm 2, \dots$

It is convenient to rewrite the conditions (19) in the form of equations for the incident and scattered angles

$$\begin{cases} \cos \alpha_f \sin \phi_f = \cos \alpha_i \sin \phi_i \\ \cos \alpha_f \cos \phi_f = \cos \alpha_i \cos \phi_i + \frac{\lambda}{l} p. \end{cases} \quad (20)$$

Therefore, if the incident radiation is perpendicular to the trenches,  $\phi_i = 0$ , then the scattered beam is also perpendicular to them,  $\phi_f = 0$ . In other words, the diffraction peaks lie in the plane  $xz$ , which proves to be the scattering plane.

For small solid angles  $\Delta\Omega$  and isotropic interface roughness, the diffuse contribution to the reflection coefficient  $R_{diff}$ , within the DWBA approach, has the form

$$\begin{aligned} R_{diff} &= \frac{1}{\sin \alpha_i} \frac{k^4}{16\pi^2} \Delta\Omega \left| \frac{\Delta \varepsilon T T'}{q_{1,z}} \right|^2 \exp \left[ -\frac{1}{2} (q_{1,z}^2 + q_{1,z}^{*2}) \sigma^2 \right] \\ &\quad \times \int_0^\infty r_\perp dr_\perp J_0(q_\perp r_\perp) (e^{i q_{1,z}^2 \langle u(\mathbf{r}_\perp) u(0) \rangle} - 1), \end{aligned} \quad (21)$$

where  $J_0(q_\perp r_\perp)$  is the Bessel function of zero order. It follows from (20) that if radiation incident perpendicular to the trenches, the diffraction peaks should be observed only when grazing angles of the incident and scattered rays are connected by the relation

$$\cos \alpha_f - \cos \alpha_i = p \frac{\lambda}{l}, \quad p = 0, \pm 1, \pm 2, \dots \quad (22)$$

If the incident radiation is not perpendicular to the trenches,  $\phi_i \neq 0$ , then the angles at which one can observe the diffraction peaks are given by the expressions arising from (20)

$$\begin{cases} \cos \alpha_f \sin \phi_f = \cos \alpha_i \sin \phi_i + \frac{\lambda p}{l \cos \alpha_i \sin \phi_i}, & p = 0, \pm 1, \pm 2, \dots \\ \cos \alpha_f \cos \phi_f = \cos \alpha_i \cos \phi_i \sqrt{1 + \frac{\lambda^2 p^2}{l^2 \cos^2 \alpha_i \sin^2 \phi_i}}. \end{cases} \quad (23)$$

These conditions imply that, if the incident radiation is not perpendicular to the trenches, i.e.,  $\phi_i \neq 0$ , then the incident and scattered rays will lie in different planes perpendicular to the interface, i.e.,  $\phi_f \neq \phi_i$ . However, if condition  $\lambda/l \ll 1$  is valid, then for small grazing angles of the incident radiation  $\cos \alpha_i \approx 1$ , and therefore the difference between angle  $\phi_f$  and  $\phi_i$  will be negligible in a wide range of angles  $\phi_i$ . Because of the large size of the entrance detector slits in a plane parallel to the interface, the diffraction pattern will be observable for relatively large sample turns around the  $z$ -axis. However, it should disappear when the angle  $\phi_i$  approaches the value  $\pi/2$ , i.e., for the case, when the trenches are parallel to the plane perpendicular to the interface, which contains the incident beam. This is indeed what has been observed in the experiment, see Fig. 5.

The diffraction peaks and the contribution of diffuse scattering are observed usually in experiments of two types. In the first of them, the sample is rotated, whereas the source and the detector are fixed. In the second type of experiment, the detector is moved, while the position of the source and of the sample is kept fixed. In the first case, the sample is rotated but the scattering angle  $\alpha_i + \alpha_f$  is constant. In the second type of experiment, the angle  $\alpha_f$  is changed at fixed  $\alpha_i$ .

The shape and the height of the satellite peaks depend on the difference between the permittivities of the substrate and the material filling the trenches  $|\Delta\varepsilon| = |\varepsilon_s - \varepsilon_{np}|$ . In the

case of empty trenches, we have  $|\Delta\varepsilon| = |\varepsilon_s - 1|$ . For x-ray radiation with a wavelength of 0.1541 nm, we have for the silicon substrate  $\varepsilon_s = 1 - 1.517 \times 10^{-5} + i3.465 \times 10^{-7}$ . Therefore, for the empty trenches,  $|\Delta\varepsilon|^2 = |\varepsilon_s - 1|^2 = 2.303 \times 10^{-10}$ . For trenches filled by NPs, one can estimate the average value  $\varepsilon_{np}$  as follows. The NPs are spheres with average diameter 20 nm. They are composed of iron oxide coated with a layer of oleic acid of 1 nm thickness. For the oleic acid,  $\delta$  and  $\beta$  are much smaller than for iron oxide. Therefore, even with close packing of NPs, the iron oxide occupies approximately 65% of the trench volume. This means that the trenches are filled with a medium with a permittivity of  $\varepsilon_{np} = 1 - 0.65 \cdot 2\delta_{FeO} + i \cdot 0.65 \cdot 2\beta_{FeO}$ . If we take the following values,  $\delta_{FeO} = 2.313 \times 10^{-5}$  and  $\beta_{FeO} = 2.281 \times 10^{-6}$  for the real and imaginary parts, respectively, we will obtain  $|\Delta\varepsilon|^2 = |\varepsilon_s - \varepsilon_{np}|^2 = 2.288 \times 10^{-10}$ . It should be noted that the contrast  $|\Delta\varepsilon|$  for empty trenches and for trenches filled with iron oxide NPs is almost the same. This leads to coinciding x-ray scattering intensities for systems with empty and filled trenches with nanoparticles (see Figure 9(a)). The choice of a different material or other volume fractions of the NPs would lead to a different contrast value  $|\Delta\varepsilon|$  and thus to other scattering intensities for the satellite peaks, as shown in Figure 9(b).

#### IV. CONCLUSIONS

In this contribution, we have investigated by x-ray scattering periodic arrays of trenches etched in silicon substrates. The trenches were filled by spin-coating with FeO magnetic nanoparticles. The aim of the study was to determine from the x-ray intensity of the satellite peaks before and after spin coating the filling factor of the trenches. Experimentally, we measured basically no difference in the intensity. From a theoretical analysis of the scattering intensity within the distorted wave Born approximation, it turns out that the condition of equal intensity before and after filling is met for a volume fraction of about 65% of FeO. For higher or lower volume fractions, an intensity difference is expected between the empty and filled trenches. This filling factor is in perfect agreement with the one that we obtain for spin-coating of FeO nanoparticles on plane Si substrates.<sup>9</sup> Moreover, the templates reduce the defects and disclinations as evident from the SEM images. Fluctuations of the trench periodicity, trench wall thickness, and/or depth of the trenches lead to diffuse x-ray scattering. This becomes noticeable at small incident angles. At higher scattering angles, the sensitivity to the array of trenches is being lost. Thus, the best probing angle for the x-ray analysis of the trench pattern turns out to be intermediate between glancing angles and higher angles, and is about  $2^\circ$  for the present experiments with x-ray wavelengths between 0.11 nm and 0.15 nm.

#### ACKNOWLEDGMENTS

One of us (DM) gratefully acknowledges support from the NRW Graduate School: "Research with synchrotron radiation in the nano- and biosciences," Dortmund and from the Ruhr-University Bochum through the Research Department

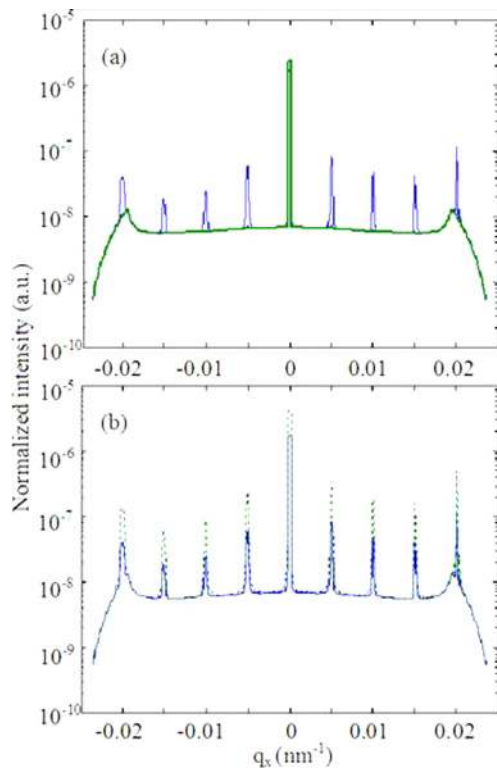


FIG. 9. Calculated rocking scans for systems with empty trenches and trenches filled with nanoparticles. Panel (a): Solid blue line corresponds to empty trenches or to trenches with 65% volume fraction of FeO nanoparticles. Green line corresponds to 33% volume fraction of FeO in trenches. Panel (b): Solid blue line has the same meaning as in (a). Dashed green line corresponds to 100% volume fraction of FeO in the trenches. In all cases, calculations are provided at  $2^\circ$  of detector angle, for an x-ray wavelength of  $\lambda = 0.1541$  nm, and assuming that the trenches are oriented perpendicular to the scattering plane.

IS3/HTM. The authors also gratefully acknowledge beam time allocation and support by the HASYLAB at DESY Hamburg and DELTA synchrotron at the University of Dortmund. This work was partially supported by DFG-RFBR cooperative Grant DFG: No. ZA 161/20-1 and Grant RFBR No. 13-02-01255A.

- <sup>1</sup>G. Reiss and A. Hütten, *Nature Mater.* **4**, 725–726 (2005).  
<sup>2</sup>M. Grzelczak, J. Vermant, E. M. Furst, and L. M. Liz-Marzan, *ACS Nano* **4**, 3591–3605 (2010).  
<sup>3</sup>S. Disch, E. Wetterskog, R. P. Hermann, D. Korolkov, P. Busch, P. Boesecke, O. Lyon, U. Vainio, G. Salazar-Alvarez, L. Bergström, and T. Brückel, *Nanoscale* **5**, 3969 (2013).  
<sup>4</sup>G. A. B. Confalonieri, V. Vega, A. Ebbing, D. Mishra, P. Szary, V. M. Prida, O. Petravic, and H. Zabel, *Nanotechnology* **22**, 285608 (2011).  
<sup>5</sup>M. J. Benitez, “Self-assembled magnetic nanostructures: Synthesis and characterization,” Ph.D. thesis (Ruhr University, Bochum, 2009).  
<sup>6</sup>B. J. Bang, U. Jeong, D. Y. Ryu, T. P. Russell, and C. J. Hawker, *Adv. Mater.* **21**, 4769 (2009).  
<sup>7</sup>G. Singh, S. Pillai, A. Arpanaei, and P. Kingshott, *Nanotechnology* **22**, 225601 (2011).  
<sup>8</sup>H. Li, J. D. Carter, and T. H. LaBean, *Mater. Today* **12**, 24 (2009).  
<sup>9</sup>D. Mishra, M. J. Benitez, G. A. B. Confalonieri, P. Szary, F. Brüßing, O. Petravic, K. Theis-Bröhl, A. Devishvili, A. Vorobiev, O. Kononov, M. Paulus, C. Sternemann, B. P. Toperverg, and H. Zabel, *Nanotechnology* **23**, 055707 (2012).  
<sup>10</sup>K. Nygard, D. K. Satapathy, O. Bunk, E. Perret, J. Buitenhuis, C. David, and J. F. van der Veen, *J. Appl. Cryst.* **42**, 1129 (2009).  
<sup>11</sup>O. Bunk, A. Diaz, F. Pfeiffer, C. David, B. Schmitt, D. K. Satapathy, and J. Friso van der Veen, *Acta Cryst. A* **63**, 306–314 (2007).  
<sup>12</sup>G. T. Baumbach and M. Gailhanou, *J. Phys. D: Appl. Phys.* **28**, 2321 (1995).  
<sup>13</sup>P. Mikulik and T. Baumbach, *Phys. Rev. B* **59**, 7632 (1999).  
<sup>14</sup>M. Tolan, W. Press, F. Brinkop, and J. P. Kotthaus, *J. Appl. Phys.* **75**, 7761 (1994).  
<sup>15</sup>M. Tolan, W. Press, F. Brinkop, and J. P. Kotthaus, *Phys. Rev. B* **51**, 2239 (1995).  
<sup>16</sup>U. Pietsch, V. Holý, and T. Baumbach, *High-Resolution X-Ray Scattering: From Thin Films to Lateral Nanostructures*, 2nd ed. (Springer-Verlag, New-York, 2004).  
<sup>17</sup>M. J. Benitez, D. Mishra, P. Szary, G. A. B. Confalonieri, M. Feyen, A. H. Lu, L. Agudo, G. Eggeler, O. Petravic, and H. Zabel, *J. Phys.: Condens. Matter* **23**, 126003 (2011).  
<sup>18</sup>F. Luo, L. J. Heyderman, H. H. Solak, T. Thomson, and M. E. Best, *Appl. Phys. Lett.* **92**, 102505 (2008).  
<sup>19</sup>S. K. Sinha, E. B. Sirota, S. Garoff, and H. B. Stanley, *Phys. Rev. B* **38**, 2297 (1988).